Tectonophysics 861 (2023) 229905

Contents lists available at ScienceDirect

Tectonophysics

journal homepage: www.elsevier.com/locate/tecto

Spatially heterogeneous lithospheric architecture of the Cambay rift basin and adjoining Aravalli-Delhi Fold Belt, western India – A synthesis of magnetotelluric results

Danda Nagarjuna[a,b,*], Amit Kumar[c], G. Pavankumar[a], C.K. Rao[b,d,1], Ajay Manglik[a]

[a] CSIR-National Geophysical Research Institute, Hyderabad 500 007, India
[b] Dr. K.S. Krishnan Geomagnetic Research Laboratory, IIG, Prayagraj 221505, India
[c] Indian Institute of Geomagnetism, Navi Mumbai, 410218, India
[d] B503/504, Aspen, Adhiraj Gardens, Navi Mumbai - 410210, India

ARTICLE INFO

Keywords:
Cambay rift basin
Aravalli-Delhi Fold Belt
Magnetotellurics
Electrical conductivity
Réunion plume

ABSTRACT

The Cambay rift basin (CRB) evolution has been associated with separation of the Indian continent from the African continent and subsequent interaction with the Réunion mantle plume, which resulted in significant alternations in the regional lithospheric structure of western India, more prominently in the CRB due to its proximity to the plume track. In our continued effort to delineate the lithospheric structure of the CRB and adjoining regions, we acquired magnetotelluric (MT) data at 31 sites along a profile across the CRB and analyzed these. The 2D geoelectric model derived from this dataset reveals a collage of conductive and resistive formations. The resistive blocks indicate the Archaean lithosphere on the west, the uplifted crust within the CRB, and various structural units of the Precambrian Era on the east providing evidence for continuation of the Aravalli-Delhi Fold Belt trend beneath the CRB into Saurashtra. The conductive anomalies beneath the CRB infer the magmatic underplating associated with thermal influx derived from the upper mantle as a result of the Réunion plume interaction. Integration of previous geophysical and present results infers a spatially heterogeneous lithosphere possibly representing an assemblage the Archaean and Proterozoic lithospheres beneath the CRB. The Proterozoic lithosphere is more vulnerable to the impact of the Réunion plume due to its weak nature in comparison to the Archaean lithosphere. The Archaean lithosphere on the western side of CRB indicates initial stage of rifting, whereas Proterozoic lithosphere infers second stage coeval with the Deccan volcanic eruption. The heterogeneity in sedimentary thickness within the CRB spatially correlates with the contact of Archaean and Proterozoic lithospheres, which might have played a role in the formation of the basin structure, and sediment deposition.

1. Introduction

Plume–lithosphere interactions, continental collision, and rifting are demonstrated as major geophysical processes that cause changes in the lithospheric structural configurations (McKenzie, 1985; Griffiths and Campbell, 1990; Saunders et al., 1992; Dewey et al., 1993; Meissner et al., 1991). These interactions also result changes in the thermal and physical properties of the subsurface structures, establishing the presence of magma chambers at upper mantle depths. These magma chambers play a significant role in volcanic eruptions as witnessed in the Indian sub-continent. The geodynamic history of the Indian sub-continent is mainly associated with departures of Africa, Antarctica and Australia, Madagascar, and Seychelles during the ages of ~180–64 Ma (e.g., Mahoney et al., 1991; White and McKenzie, 1989). These events have caused rifting and large-scale magmatism. The magmatism beneath the Indian plate has been attributed to the influence of four mantle plumes, the Crozet, Marion, Kerguelen, and Réunion, during its northward drift (Morgan, 1971, 1981; Watts and Cox, 1989). The interaction of the Réunion mantle plume and Indian continental lithosphere has resulted in a huge volcanic eruption in a short period of <1 Myr at western India ~65 Ma, which is now manifested as the Deccan volcanic province (DVP) (Duncan and Pyle, 1988; Bhatacharji et al.,

* Corresponding author at: Room Nr. 113, Main Building, CSIR-National Geophysical Research Institute, Uppal Road, Hyderabad 500007, India.
E-mail address: nagarjunadanda@gmail.com (D. Nagarjuna).
[1] Retired from service

https://doi.org/10.1016/j.tecto.2023.229905
Received 7 December 2022; Received in revised form 28 April 2023; Accepted 5 May 2023
Available online 15 May 2023

1996; Raval and Veeraswamy, 2000; Veeraswamy and Raval, 2004).

The western continental margin of India (WCMI) is a structural mosaic with three marginal rift basins of India, namely, Cambay, Kachchh, and Narmada rifts (hereafter CRB, KRB, and NRB, respectively). The Réunion mantle plume would have initially affected the northwestern parts of the Indian subcontinent, particularly these marginal rifts of western India. The CRB evolution has taken place in two stages. The initial rifting is associated with the separation of the Indian and the African plates at the Late Triassic/ Early Jurassic (Biswas, 1982, 1987) and then it became a failed rift arm (Burke and Dewey, 1973; Biswas, 1982, 1987). In the next episode, India and Seychelles together got detached from Madagascar around 90 Ma and drifted in the NNE direction (Biswas, 1982, 1987). During this drift, the Indian plate was impacted by the Réunion mantle plume, producing extensional stresses, resulting in the breakup of the Indian sub-continent from Seychelles. The second stage of CRB rifting is considered to be coeval with the Deccan volcanic eruption at ~65 Ma. Seismic tomography studies attributed the presence of low-velocity anomaly at a depth range of 80–200 km to the emplacement of plume material through the lithosphere beneath the CRB (Kennett and Widiyantoro, 1999).

Previous MT studies across the CRB have postulated the assemblage of Archaean and Proterozoic lithospheres geological contact beneath the CRB and weak Proterozoic lithosphere facilitated the channelization of plume-derived fluids/melts into the crustal depths (Danda et al., 2017, 2020, 2021). Further, these studies also highlighted the heterogeneous lithospheric structures beneath different parts of the northern CRB. Various geophysical studies infer the extensions of Delhi trend into the KRB, Aravalli trend into the Saurashtra beneath the CRB (Biswas, 1982, 1987; Tewari et al., 1991). The deep seismic sounding (DSS) and gravity studies provide evidences for crustal thinning, underplating and also infer the presence of various ridges and depressions separated by transect basement faults within the CRB (Kaila et al., 1981, 1990; Mishra et al., 1998). To understand the nature of heterogeneities in the basement, crustal, and lithospheric structures beneath the CRB and the impact of the Réunion mantle plume, a new MT profile with a total of 31 MT sites was acquired across the CRB and neighboring Aravalli-Delhi fold belt (ADFB) (Fig. 1). In this paper, we have made a synthesis of geophysical results by integrating the new MT with previous MT results, and compared with the Deep seismic sounding (DSS), gravity results along the CRB. The synthesis of geophysical results over the CRB provide the evidences for westward extension of Aravalli-Delhi trends, basement heterogeneities, better understanding of the geodynamic evolution process, and lithospheric structural architecture of the CRB.

2. Geology and tectonics

The CRB is a major hydrocarbon producing basin in western India, located between 21°N and 24°30'N latitudes and 71°30'E and 73°45'E longitudes. The NNW-SSE oriented CRB extends to the Barmer basin in the North and the Gulf of Cambay in the South into the Arabian Sea. The CRB is wider in the South and becomes narrow towards the North in the Sanchore region. The CRB is bordered by the ENE-WSW oriented KRB in the north, the ENE-WSW oriented NRB in its south, and the Saurashtra Peninsula sheltered by Deccan traps of late Cretaceous age in the West. Towards the east, it is bounded by the Aravalli system comprising of older Proterozoic rocks of Aravalli and Delhi Supergroups (Merh, 1995). Various geophysical studies inferred that the Aravalli trend (NE-SW) extends further southwest beneath the CRB into the Saurashtra

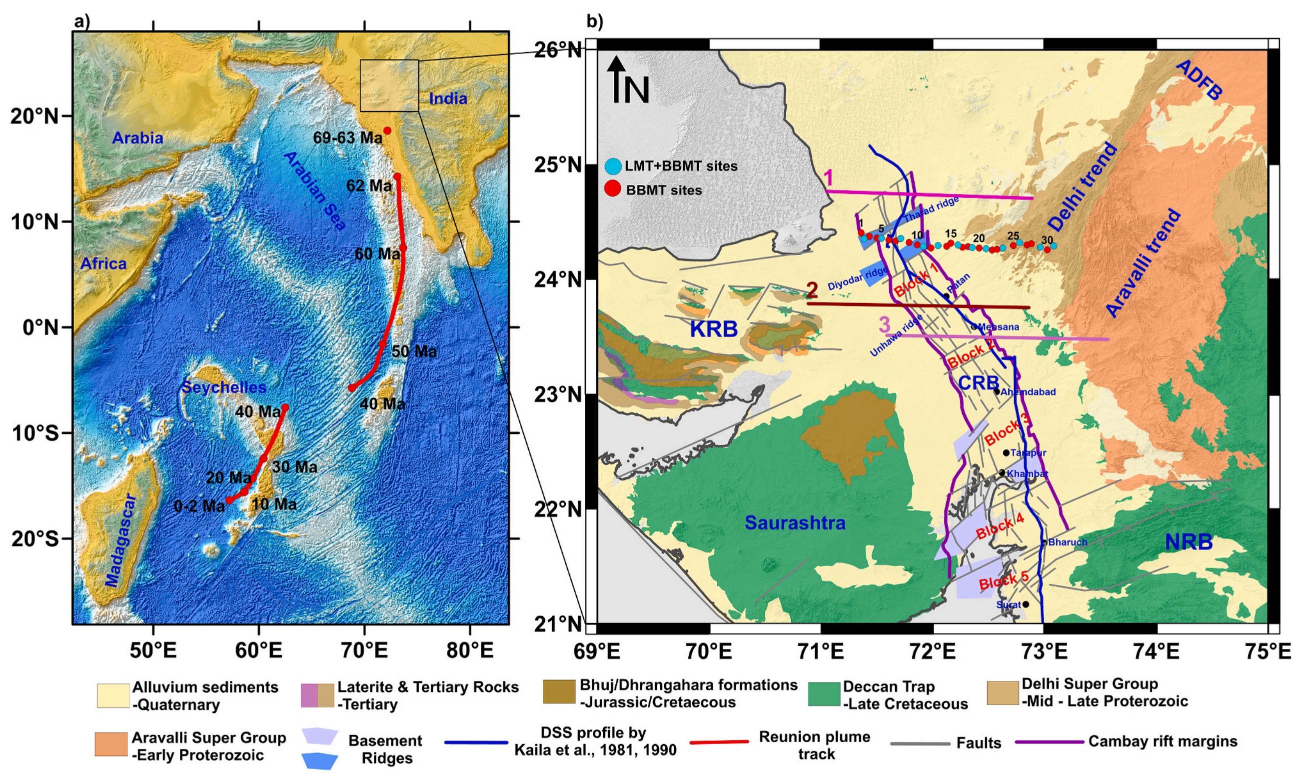

Fig. 1. a) The Reunion mantle plume track and different continental fragments of Gondwanaland. (Bathymetry data source: GEBCO Compilation Group, 2021) b) Regional geological and tectonic map of the western India superimposed on the background of topography from the SRTM data (http://dds.cr.usgs.gov/srtm/version 2_1/SRTM30//srtm30; modified from Biswas, 1982, 1987; Mishra et al., 1998; Danda et al., 2017, 2020). Geological domains, major faults are from the shape files available at the BHUKOSH portal of Geological Survey of India (http://bhukosh.gsi.gov.in/Bhukosh/MapViewer.aspx). The different colours of solid lines represent previous MT profiles, 1: Danda et al., 2017; 2: Danda et al., 2021; 3: Danda et al., 2020. The DSS profile is represented by solid blue colour (Kaila et al., 1981, 1990). CRB-Cambay rift basin, KRB-Kachchh rift basin, NRB-Narmada rift basin, ADFB-Aravalli-Delhi fold belt. Sub blocks of CRB: Block 1: Patan-Sanchore, Block 2: Ahmedabad-Mehsana, Block 3: Cambay-Tarapur, Block 4: Jambusar-Broach, Block 5: Narmada-Tapti. (For interpretation of the references to colour in this figure legend, the reader is referred to the web version of this article.)

peninsula, whereas the Delhi trend (NE-SW) swings approximately in an E-W direction under the KRB (Mishra et al., 1998; Tewari et al., 1991).

Several deep-seated faults divide the CRB into different blocks, viz. Patan-Sanchore, Ahmedabad-Mehsana, Cambay-Tarapur, Jambusar-Broach, Narmada-Tapti (Fig. 1). Each block behaved differently according to its movement along different faults within the rift basin. These blocks are filled with Tertiary and Quaternary sediments. The drilled wells in the CRB have penetrated the fluvio-deltaic sedimentary sequence of the Lower Cretaceous age (Biswas, 1982). The *syn*-rift stage in the Paleocene is characterized by alluvial and thick volcano-clastic sediments, lacustrine claystones were deposited in the Tertiary sequence in fault controlled half-grabens (Biswas, 1982, 1987). In the subsidence stage, dark shales were deposited through marine sedimentation during an Early Eocene transgressive cycle and followed by deltaic and lagoonal sedimentation in intra-basinal lows during oscillatory stages. In the Miocene, the rocks of the CRB were covered by thick alluvial sedimentary deposits deposited during extensive marine transgression events. Seismic studies across the CRB inferred that the Mesozoic sediments (thickness ~ 1.2 km) may be present beneath the Deccan traps and these form basement for the overlained Tertiary sedimentary sequence of ~5 km thickness (Biswas, 1982). The Deccan volcanic eruption has also brought stratigraphic changes across the CRB. The stratigraphic sequence is a Precambrian basement overlain by Mesozoic sediments followed by thin Deccan traps and then thick Tertiary and Quaternary sediments at the top (Biswas, 1987).

3. MT field studies

3.1. Data acquisition and processing

We acquired broadband (320 Hz–3000 s) and long-period (1–30,000 s) MT data in 2012 at 31 sites across the northern part of the CRB and ADFB in a remote reference mode to reduce local biasing effects for high quality data (Gamble et al., 1979). Long-period MT (LMT) data for ~4 weeks duration at each site were acquired by using LEMI-417 instruments at 12 sites with station interval of ~15–20 km. Broadband MT (BBMT) data for ~40 h duration at each site were acquired using the Phoenix Geophysics MTU-V5 systems with a station spacing of ~5–8 km (Fig. 1). The two horizontal electric field components (E_x and E_y) were measured by using two sets of Pb/$PbCl_2$ electrodes in the North-South and East-West directions with a dipole length of 60 m. Induction coils and ring-core fluxgate magnetometers were utilized for recording the orthogonal magnetic field (Hx, Hy, and Hz) variations in BBMT and LMT data, respectively. The acquired BBMT and LMT time series data were processed by using SSMT 2000, LEMIMT software packages, respectively based on robust reference cascade decimation techniques (Jones and Jödicke, 1984; Jones et al., 1989; Varentsov et al., 2003; Chave and Thomson, 2004). Both the BBMT and LMT datasets (at 12 sites) were merged to obtain the response estimates that were subsequently converted to apparent resistivities and phases over a period range of 0.0026–30,000 s. The noisy tipper data (calculated from vertical magnetic field (Hz) and horizontal magnetic fields (Hx, Hy)) were omitted at a few frequencies at all the sites.

3.2. Dimensionality and strike analyses

Assessment of the dimensionality of MT data is an essential step in choosing the appropriate modelling/inversion scheme for the dataset. In this study, we used Phase tensor (PT) analysis (Caldwell et al., 2004) for estimating the dimensionality and directionality of the acquired MT data. The PT analysis estimates phase sensitive skew angle (β), maximum phase (Φ_{max}), minimum phase (Φ_{min}), and a directional angle (α), without any prior assumptions on the dimensionality of regional structure. The skew angle (β) is zero for an identical 2-D structure with a strike direction towards the Φ_{max} or Φ_{min}. The skew angle (β) values computed for the present profile are below ±5° indicating 2-D subsurface structure (Liang et al., 2018) with an exception at a few low, dead band frequencies on the western side and center of the profile, respectively (Fig. 2). However, one station (Site no: 30) is showing skew values higher than ±5° is highlighted with a red box is removed from further analysis and inversion.

Since the data show the 2-D nature, geoelectric strike directions are estimated using the Becken and Burkhardt tensor (BB) decomposition approach (Becken and Burkhardt, 2004) and PT analysis. The strike directions were computed for different bands (1–10s, 10–100 s, 100–1000s, 1000–10,000 s, and 1–10,000 s). The strike directions obtained from single-site and multifrequency for the bands, 1–10s, 100–1000s, and 1–10,000 s are showing a strike angle of N50° ± 5°E, whereas other bands 10–100 s, 100–1000s show scattered strike angle between N30°E to N50°E (Fig. 3). The multisite and multifrequency analysis of BB approach for the period range of 1–10,000 s estimated the strike direction of N53°E, which correlates with the strike angles calculated for the individual bands through the BB approach. The PT analysis is also used to estimate the strike angle for various bands of MT data (1–10s, 10–100 s, 100–1000s, 1000–10,000 s and 1–10,000 s). Similar to the BB approach, PT analysis has shown similar strike angles (N50° ± 5°E) for the individual bands 1–10s, 100–1000s, while the other bands 10–100 s, 100–1000s showed scattered strike angles (Fig. 3). The PT analysis for the period band 1–10,000 s shows a strike angle scattered between the N30°E to N70°E. By considering the dominant trend from both BB and PT analysis, N53°E is considered as the regional strike direction for the present profile, which corroborates with the ADFB trend. On the basis of estimated strike angle, the impedance tensors are rotated into geoelectric strike coordinates by decomposing the data into TE and TM modes. The decomposed impedance tensors are represented as apparent resistivity and phase curves at some sites are shown in Fig. 4.

3.3. Two-dimensional inversion and sensitivity analysis

The nonlinear conjugate gradient (NLCG) algorithm of Rodi and Mackie (2001) implemented in the WinGLink software package was used to invert the decomposed TE- and TM-mode responses to obtain the plausible lithospheric electric structure across the CRB and ADFB in terms of electrical resistivity variations. The NLCG algorithm utilizes a nonlinear conjugate gradient to minimize the model misfit and produce the smoothest model from a homogeneous half-space with the combination of various inversion parameters (squared Laplacian, a smoothing term, horizontal and vertical resistivity gradients). This algorithm is based on a non-uniform grid finite difference method and allow to invert the data under the consideration of topography. We utilized a homogeneous half-space model of 100 Ωm resistivity as an initial guess model with dimensions of 78 rows (depth) and 178 columns (profile distance). After a few iterations, the grid was refined in both horizontal and vertical directions to 97 rows and 202 columns by making fine, coarse grids in shallow and deeper depths, respectively in the regions showing sharp variations in the electrical resistivity in the model at boundaries/contact zones corresponding to different structures. The horizontal and vertical gradients describing the block dimensions were set as 500 m, and horizontal (α) and vertical (β) smoothing parameters are taken as 1. The error floors for 20% and 10% for apparent resistivities, 10% (2.9°) and 5% (1.45°) for phases of TE- and TM-mode, respectively, and 0.025 for Tipper (Hz) data were considered in the inversion scheme. Higher error floor in the TE- over TM-mode helps to reduce the plausible inherent effects of localized heterogeneities and static shift in the data (e.g. Jones, 1983; Wannamaker et al., 1984; Ledo et al., 2002; Ogawa, 2002; Ledo, 2005). Tipper data were included in the inversion scheme after 50 iterations to avoid the underfitting of data due to its inherent sensitivity to conductive anomalies rather than the conductivity of half-space (Rao et al., 2014; Danda et al., 2020). The regularization parameter (τ) describes the trade-off between the model misfit and roughness is a significant parameter in the inversion scheme. The value of this parameter was considered as 7 after various experimental inversion runs. Though

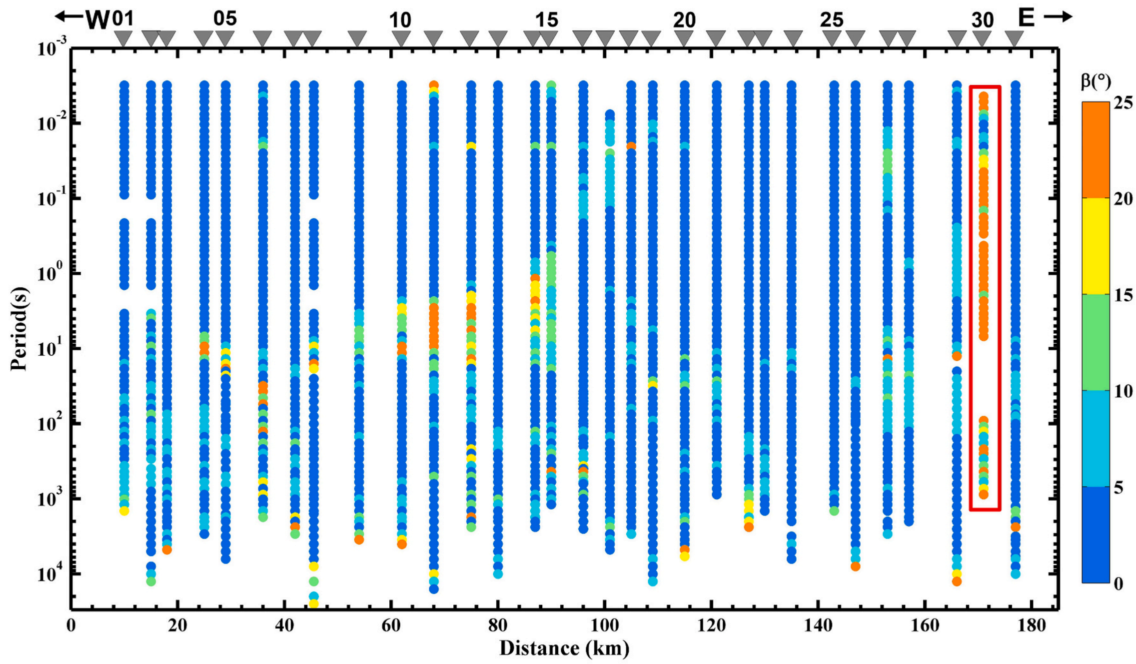

Fig. 2. Graphical representation of phase tensor skew angle (β) computed from the Phase tensor analysis for all sites of the profile. A red box on the site no: 30 show skew values >5° may indicate 3D nature, and this data is discarded from further analysis and inversion. (For interpretation of the references to colour in this figure legend, the reader is referred to the web version of this article.)

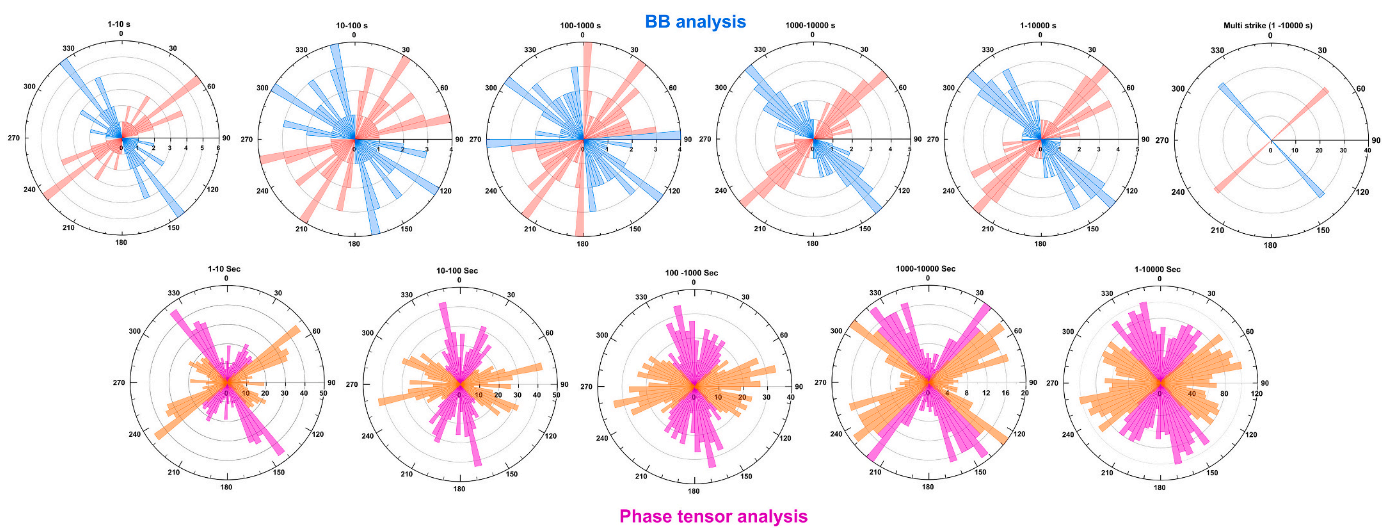

Fig. 3. Rose diagrams showing dominant geoelectric strike directions. Top row diagrams represent the directions computed by the Becken and Burkhardt (BB) analysis (Becken and Burkhardt, 2004) for different period bands. Bottom row diagrams represent the directions computed by the Phase tensor analysis (Caldwell et al., 2004). (For interpretation of the references to colour in this figure legend, the reader is referred to the web version of this article.)

the inversion scheme allows for the inclusion of topography, it is not included since the topography along the profile varies from ~50–400 m only (Fig. 5a). The effects arising from this range may be negligible (Pavankumar and Manglik, 2011). The final resistivity model for the MT profile across the CRB and ADFB obtained from simultaneous inversion of TE- and TM-modes apparent resistivity and phases, and tipper data is shown in Fig. 5b. The final model (Fig. 5b) is obtained after 180–200 iterations with a final RMS error of 1.936.

In general, the initial model may give rise to artifacts in the insensitive and unresolved parts of the model. To understand the effects of the initial half-space model and for robust estimation of the final model, inversions with 10 Ωm and 1000 Ωm half-space models were conducted by keeping other parameters used in 100 Ωm unchanged. The resulting geoelectrical models from 10 Ωm and 1000 Ωm half-space models showed similar structures as obtained from the 100 Ωm half-space model and it can be considered as a robust model (Fig. S1, supplementary information). Prior to analyzing the structural features in the model (Fig. 5b), it is important to estimate the robustness of individual features in the model. For this, we followed constrained inversion approach to test the robustness of major resistive (R1-R4) and conductive (C1-C6), upper mantle conductor (UMC) features in the model (Pavankumar et al., 2014; Adilakshmi et al., 2021). In the constrained inversion, the resistive feature (R1) was replaced with the half-space resistivity (100 Ωm), and inversion was carried out for the altered resulting model with the same model parameters used for the model shown in Fig. 5b. The resistive block R1 is reproduced through the constrained inversion after

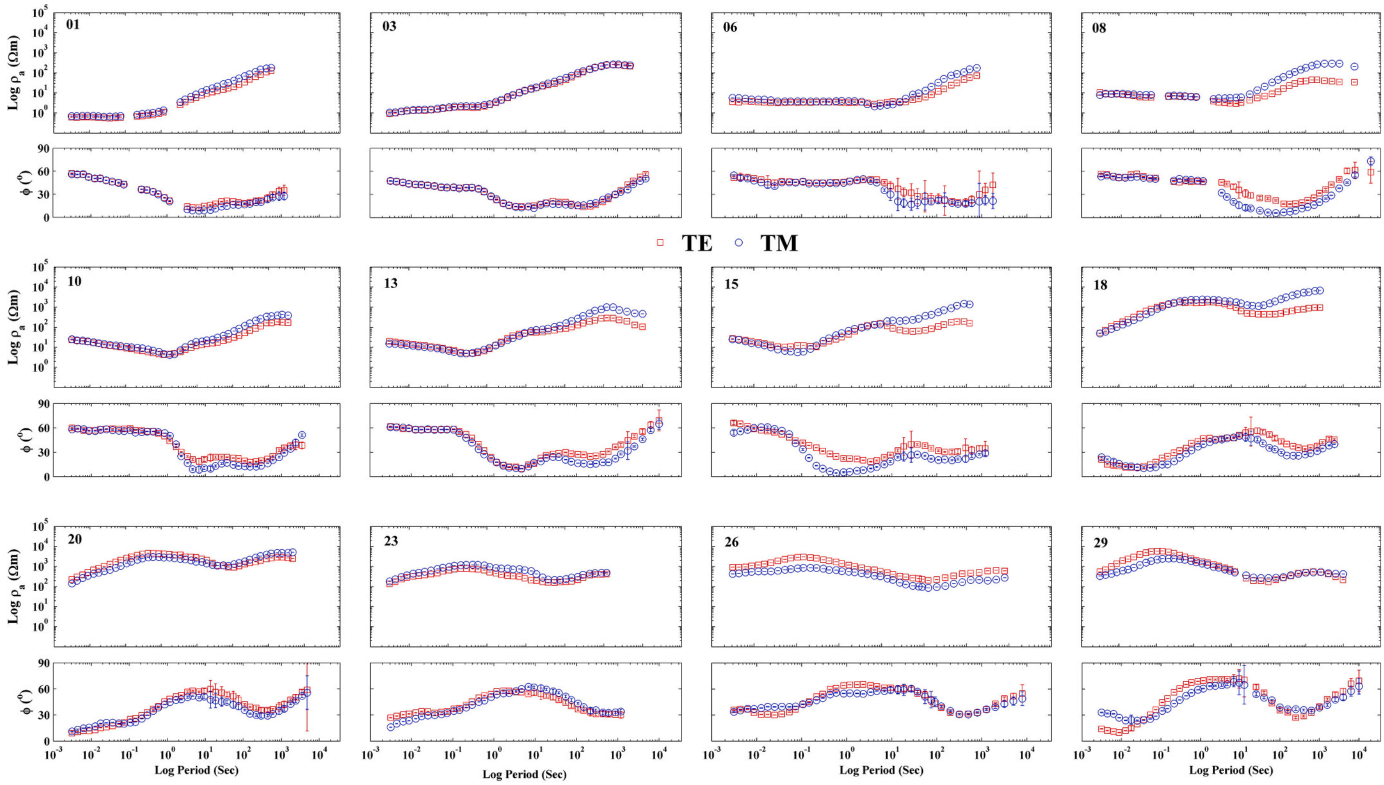

Fig. 4. Apparent resistivity and phase curves for representative stations of data used in 2D inversion from MT profile across the CRB and ADFB. The red colour squares represent TE mode and the Blue colour circles represent TM mode. (For interpretation of the references to colour in this figure legend, the reader is referred to the web version of this article.)

50 iterations. Likewise, the constrained inversion was executed for other major features (C1-C6, UMC; R2-R4) independently and all features are reproduced after 50 or more iterations (Fig: S2-S3, supplementary information). The NLCG algorithm allows to compute the sensitivity matrix by establishing a first order approximation on how a perturbation of model parameters can affect the computed model measurements and also provides an information about both uncertainty and resolution of the computed models (Fig. 5b) on the basis of Mackie et al. (1997) and it is showed in Fig. 5c. The major resistive (R1-R4) and conductive (C1-C6, UMC) structures in the model show higher sensitivity values >0.0001, infer the robustness of these structures (e.g., Brasse et al., 2002; Schwalenberg et al., 2002; Ledo et al., 2004; Schmoldt et al., 2014). In summary, by considering the robustness from different half-space models, constrained inversion, and sensitivity matrix, the model features in Fig. 5b are robust in nature. Pseudo-sections of observed and modelled apparent resistivity and phase data for TE- and TM-modes, and tipper data are shown in Fig. 6 to indicate the best fit between observed and computed responses of TE- and TM-mode data. The misfit in tipper data mainly arises due to the removal of noisy data at few frequencies at all the sites. In such cases, it mainly extrapolates calculated response from the model where data is absent. In such cases a small misfit in the data looks like significant misfit in entire Hz data since it extrapolates such misfit where data is absent. The misfits in the tipper data is due to removal noisy data points in the original data. The fitting between observed and computed responses of apparent resistivity and phases of TE- and TM-modes for individual sites are presented in the supplementary information.

4. Results and discussion

The final geoelectrical model (Fig. 5b) is a collage of resistive (R1-R4), conductive (C1-C6), and an upper mantle conductive (UMC) features across the CRB and ADFB down to 100 km depth. The geological domain boundaries are shown at the top of the final model (Fig. 5b). The Bouguer gravity anomaly and its gradient, and topographic elevation along profile is showed on top of final model (Fig. 5a). A thick shallow conductive layer (C1) is delineated beneath the CRB. Broadly, the model from site 11 to site 31 is dominantly resistive with a few conductive anomalies beneath the ADFB. A high resistive structure (R1) beneath the CRB is delineated at ~10 km depth with ~20 km lateral extent and it further extends into 100 km deep lithosphere and becomes much broader >40 km. Interestingly, three major crustal conductors (C2-C4) are mapped at sub-crustal depths beneath the sites 1–15. A moderate upper mantle conductor (UMC) is mapped beneath the center of the profile and merges with the crustal conductors (C3, C4).

The final model (Fig. 5b) and geoelectric models from previous magnetotelluric studies across the CRB (Danda et al., 2017, 2020, 2021) were re-gridded with the model resistivities on log10ρ scale and smoothed the grid values by applying one-pass 3-node Gaussian filter. We have extracted the resistivity values at various depths (e.g., 1, 2, 5, 10, 20, 30, 40, and 50 km) and contoured the resistivity values (Fig. 7). The seismic velocity, density values obtained from the DSS and gravity modelling along strike of the CRB are marked at the intersecting locations of the MT profiles (Fig. 7). We further discuss in detail the possible causes for the occurrence of conductive (C1-C6) and resistive (R1-R4) formations by integrating the existing geophysical information for better understanding of various subsurface processes.

4.1. Sediment thickness and basement structure

The shallow conductive layer (C1) infers the Cenozoic (Quaternary and Tertiary) sediment thickness deposited through various marine transgression events (Fig. 5b). The hydrocarbon reserves of the CRB resulted in extensive geological and geophysical exploration activities, producing detailed shallow subsurface information of the basin (Biswas, 1982, 1987; Kaila et al., 1990; Mishra et al., 1998; Dixit et al., 2010;

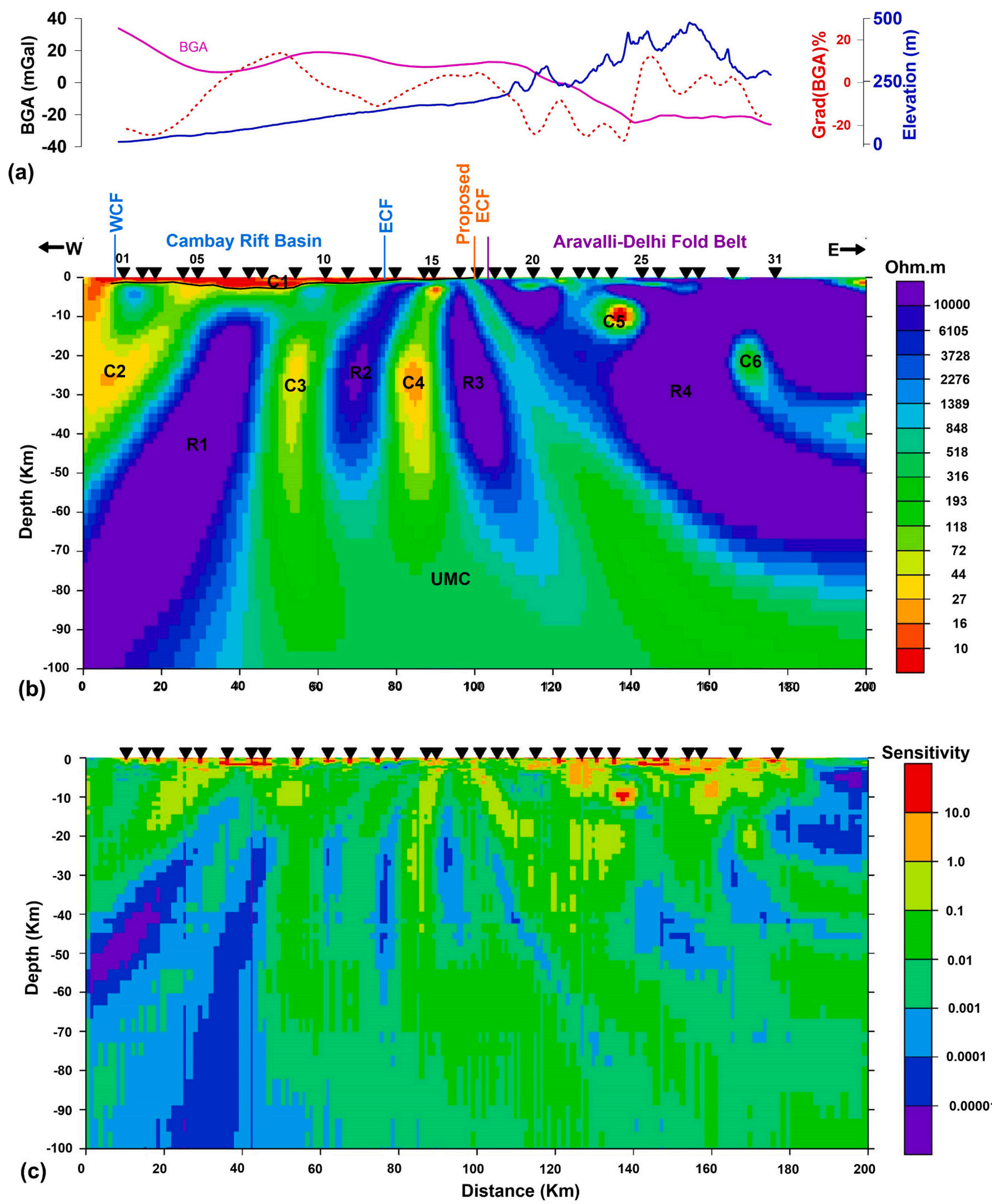

Fig. 5. a) Topographic elevation (m) along the profile. b)2-D smooth inversion geoelectric model of the MT profile across the CRB and ADFB (vertical exaggeration 1.0). The triangles indicate the location of the MT sites from west to east. Major resistive (R1-R4) and conductive features (C1-C6, UMC) are labeled. c) The sensitivity matrix values for the final geoelectric model are shown in Fig. 5b. WCF: West Cambay Fault & ECF: East Cambay Fault.

Chouhan et al., 2020 and references therein). The DSS and gravity studies along the CRB infer the presence of sediment thickness varies from ~3 km to >7 km (Kaila et al., 1990; Mishra et al., 1998). These studies further highlight the division of CRB into different blocks separated by transverse basement faults. These block moments controlled the sediment accumulation pattern, leading to variation in the sediment thickness within the CRB. The geophysical, geological studies, and Oil and Natural Gas Corporation (ONGC) well data from the CRB infer the stratigraphy as Cenozoic sedimentary sequence consisting of shales, sandstones, etc., on the top, followed by the Deccan traps underlain by the Mesozoic sediments in a few parts of the CRB. The various depressions, like Sanchore, Patan, Mehsana were developed during the subsidence of CRB accumulated thick Cenozoic sediments on the Deccan trap basement. The ONGC deep wells on the back-stripping analysis suggest different subsidence stages of the basin. Though a few stages of subsidence are associated with the India-Asia collision, various rifting phases and large subsidence occurred in the early Tertiary. Although, the CRB is developed during the Late Cretaceous, called a Tertiary basin due to the higher subsidence rate in the Tertiary. The conductive layer (C1) is thick in the centre (beneath sites: 6–9) of CRB and becomes thinner (at sites: 1–5, 9–12) on either side of it (Fig. 5b). The present profile cuts the Tharad and Diyodar ridges, which spatially coincide with the thin sediments, followed by small resistive pockets in the final model (Figs. 5b & 1). These transverse ridges controlled by basement

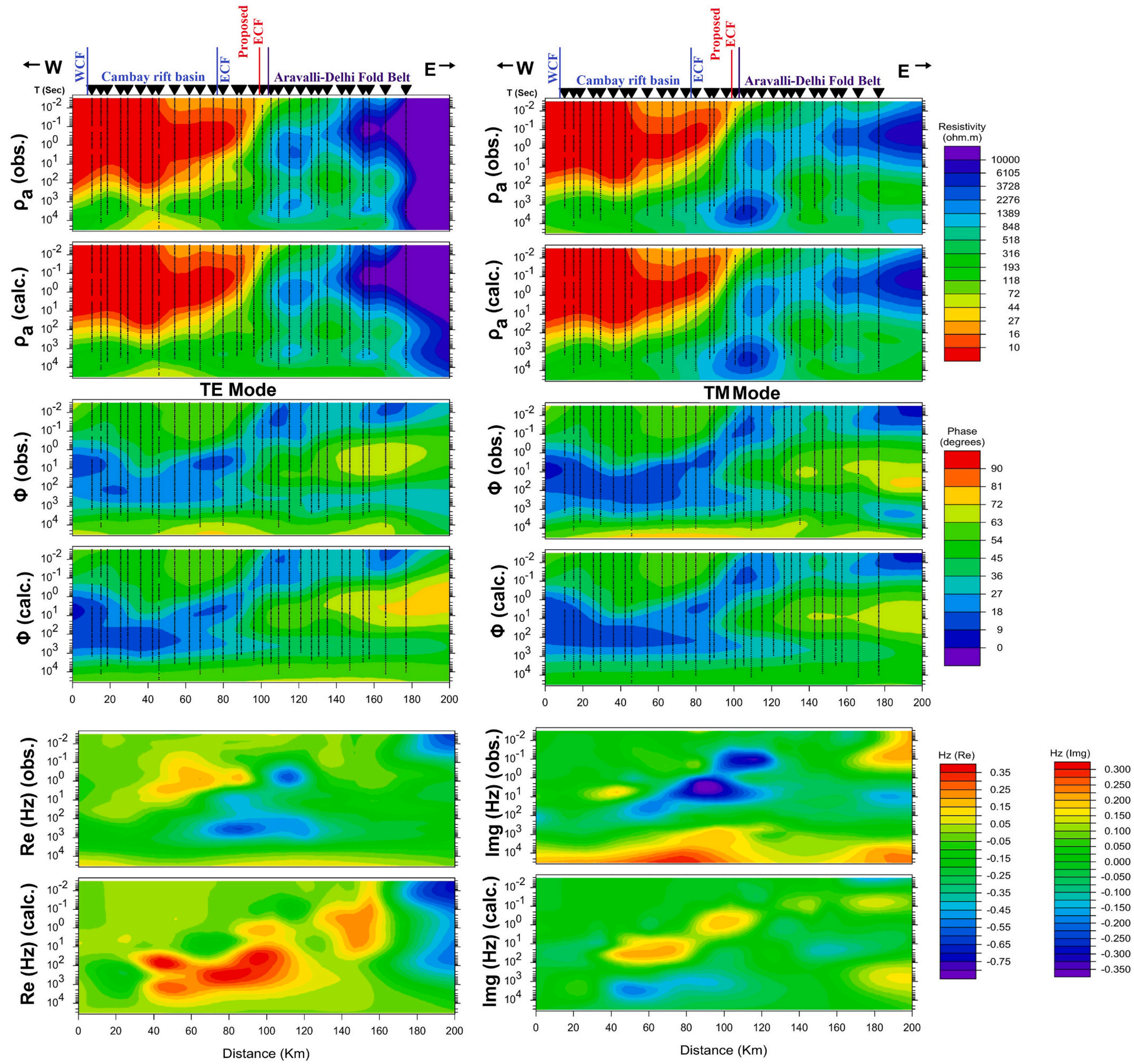

Fig. 6. Pseudo-sections showing observed and computed apparent resistivity and phase for the TE-, TM-mode, Hz real, and Hz imaginary components for the 2-D model shown in Fig. 5b. WCF: West Cambay Fault & ECF: East Cambay Fault.

faults might have caused thin accumulation of sediments on either side of the CRB. The outburst zone of Réunion plume head is located at the northern fringe of CRB (Kennett and Widiyantoro, 1999) and the extensional forces arising due to intruding volcanics lead to formation of such depressions. The high conductive zone (C1) confined to CRB at shallow depths represent the sediments-filled depression (graben) structure bounded by the parallel Tharad and Diyodar ridges. Extension of the ~1 km conductive sediments at surface, right up to the eastern margin of the CRB, may denote eastward extension of marine transgressions. Various phases of subsidence of the basin associated with the India-Asia collision and Réunion plume interaction have largely controlled the basement configuration and reactivation of basement faults (Biswas, 1982, 1987; Kaila et al., 1990; Tewari et al., 1995).

In Fig. 7, high conductivity (10 Ωm) values are observed along the basin up to 2 km depth slices, whereas variation in the conductivity values is observed at 5 km depth slices. These variations represent the different basement blocks, such as the Sanchore depression, Tharad, and Diyodar ridges, Patan, and Mehsana depressions, from north to south (Danda and Rao, 2019), which spatially coincide with the DSS and geopotential results. Low Bouguer gravity (−10 to −25 mGal) values are observed at Profiles 1,2 &3 while over the positive anomalies observed at Present study (PS) profile spatially correlate with the depressions and ridges within the CRB and corroborates with the MT results (Fig. 7). The changes in seismic velocity and density values are observed at 1–5 km depths and inferred as different layers of sedimentary formation within the CRB (Kaila et al., 1990; Mishra et al., 1998). However, the present study couldn't demarcate the individual stratigraphic units due to lack of adequate conductance contrast (Danda and Rao, 2019). The previous geophysical studies mark the eastern boundary of the CRB in between the sites 12–13. From the present study, on the basis of obtained

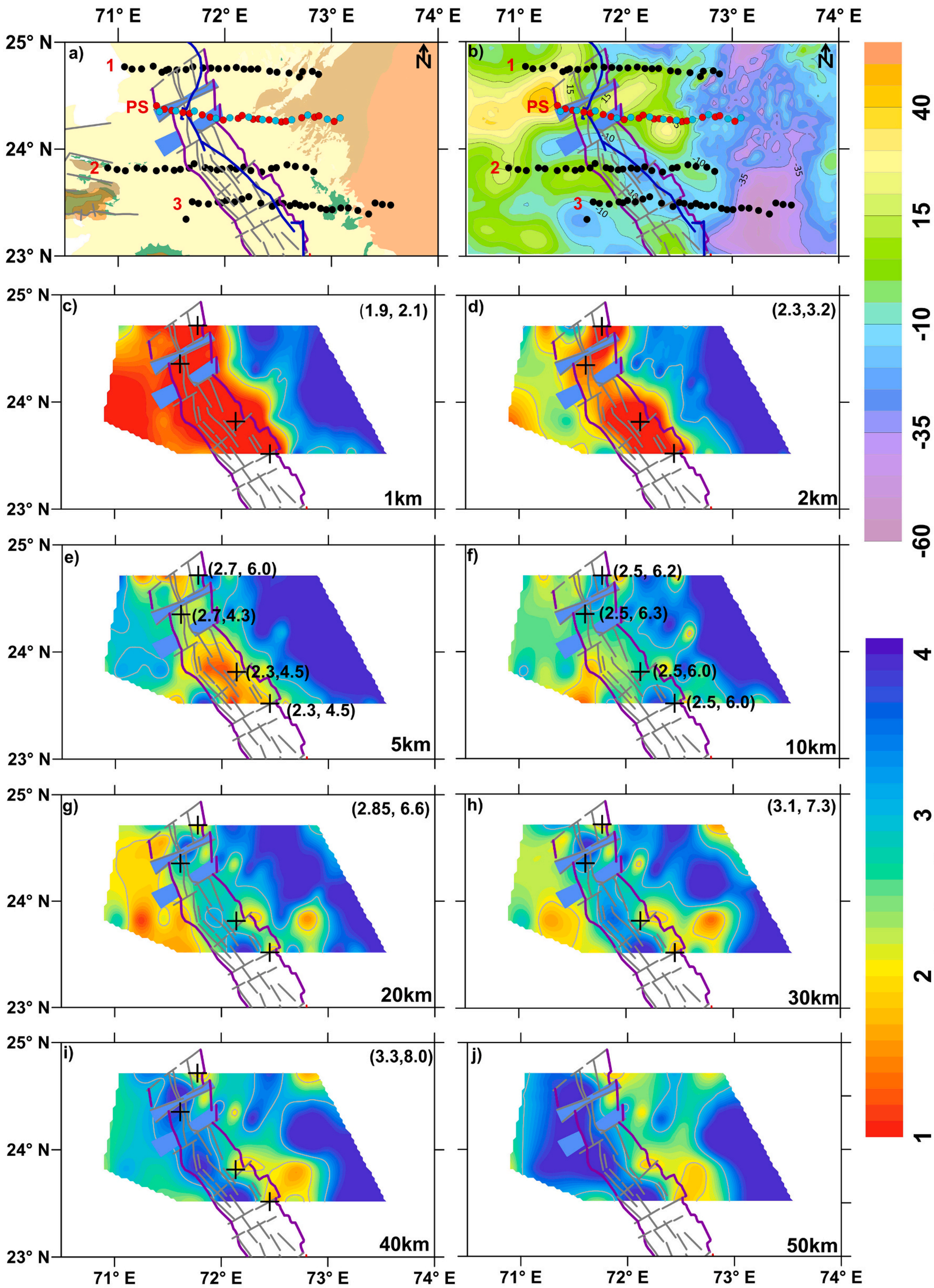

Fig. 7. a) The geological map of study area. The numbers 1,2,3 indicates MT profiles by Danda et al., 2017, 2021, 2020, respectively, and black solid circles represent corresponding MT sites. The Red and Cyan solid circles indicate BBMT and LMT sites locations of the present study (PS). Blue solid line represents the DSS profile by Kaila et al., 1990. The purple and grey solid lines represent margins the CRB and various faults within the CRB, respectively. b) Bouguer gravity contour map over the CRB. c-j) Contours of apparent resistivity at various depths, 1, 2, 5, 10, 20, 30, 40, 50 km computed from MT models across the CRB and adjoining regions. The plus (+) symbols represent intersecting locations of DSS, Gravity profiles with the MT profiles. At 1, 2, 20, 30, 40, 50 km depth slices (c-d, g-j), The seismic velocities and density values are same at the four intersecting locations and are mentioned at right corner. At 5, 10 km depth slices, the seismic velocity and density values are different at intersecting locations and the corresponding values are mentioned beside. The first number is density (g/cc) and second number is seismic velocity (km/s). (For interpretation of the references to colour in this figure legend, the reader is referred to the web version of this article.)

sediment thickness we infer that the eastern boundary might be present between the sites 16–17. Similarly, such shift in eastern boundary has been observed from the previous MT study across the Mehsana depression in the CRB (Danda et al., 2020).

4.2. Crustal and upper mantle lithospheric structure

The CRB lithospheric structure is largely unexplored though it has fairly good information on the shallow subsurface. The DSS studies conducted along the CRB to image its crustal structure inferred the average crustal thickness of 31–37 km from north to south of the basin (Kaila et al., 1990; Dixit et al., 2010). Tewari et al. (1991) made an attempt to establish a relationship between the crustal structures of the CRB with the neighboring ADFB, inferring crustal thinning within the CRB. The geopotential, heat flow, and seismological studies over the CRB have delineated a shallow Moho depth of 31–32 km with the high-density upper crust, Moho upwarp, felsic crust, the existence of intrusive bodies (Mishra et al., 1998; Gupta, 1981; Rao et al., 2015; Sharma et al., 2018; references therein). The recent MT studies (Danda et al., 2017, 2020, 2021) across the CRB and neighboring KRB and ADFB have delineated various volcanic intrusives in the crustal and upper mantle lithospheric structure of the CRB and KRB.

The present study delineates a heterogeneous crustal and upper mantle structure down to 100 km depth with a collage of conductive (C2-C4) and resistive (R1-R2) structures. The resistive structure R1 has depth extension from 10 to 100 km, similar to the resistive structures obtained beneath the western part of the CRB from previous MT studies, inferring the existence of volcanic intrusives in the crustal column, corroborating previous heat flow, geopotential, and DSS results (Gupta, 1981; Kaila et al., 1990; Tewari et al., 1991; Mishra et al., 1998). The upper mantle lithospheric portion of this resistive block infers recrystallization of depleted Archaean mantle lithosphere associated with the Réunion plume activity. The Reunion plume-lithospheric interaction may well simulate the recrystallized volcanic intrusives and it becomes shallower beneath the western part of CRB. This may favour approaching of the outburst zone of the Reunion head, which based on the MAGSAT is located close to the northern fringe of the CRB (Kennett and Widiyantoro, 1999). This stable and depleted Archaean lithosphere might represent initial stages of rifting during the Gondwana disintegration. The resistive feature R2 is possibly related to the existence of volcanic intrusives and uplifted parts of the Precambrian crust prior to Deccan volcanic eruption. On the regional scale, the Réunion plume activity gave rise to such resistive features interpreted as volcanic intrusives and traces of Precambrian crust beneath the KRB and Saurashtra (Pavankumar et al., 2017; Abdul Azeez et al., 2018; Kumar et al., 2018).

The conductive anomalies in the crustal and upper mantle lithospheric depths are the traces of deformation and underplating of magma associated with various past and current tectonic and evolution processes in the geological domain (Hyndman and Shearer, 1989; Worzewski et al., 2011; Comeau et al., 2018; Kumar et al., 2018). The evolution of the three rift basins in western India has been associated with the disintegration of Gondwanaland and the drifting of the Indian plate over the Réunion mantle plume and reactivation along the Precambrian trends (Biswas, 1982, 1987). These weak rift zones have facilitated the pathways for volcanic eruptions associated with the Réunion plume activity and resulted in the development of Deccan volcanic eruption over western and central India (Raval and Veeraswamy, 2000). The conductive anomalies (C2-C4) imaged from the present study beneath the CRB have spatial correlation with the previous MT studies. Danda et al. (2021) have imaged a trapped crustal fluidized reservoir within the KRB in the vicinity of the western margin of the CRB. The conductive structure (C2) delineated in the present model also infers the presence of fluids in the western part of the CRB crust. The electrical resistivity depth slices at 20 km and 30 km highlight the spatial correlation of the fluid reservoir in the KRB with conductive structure C2 in the CRB. The previous seismological, MT results across the KRB highlight weak fault zones in the KRB that act as pathways for the fluid transport of mantle-origin fluids into the crust and play a significant role in the seismicity of the KRB.

The Réunion mantle plume interaction with the continental lithosphere caused melting of the lithosphere and generation of melts processes of adiabatic decompression of the plume head and its corresponding thermal anomaly at the base of the lithosphere (Yardley and Bodnar, 2014). The low density and high buoyancy caused to migrate through the weak zones into the crust (Courtillot et al., 1988; Dunbar and Sawyer, 1989; Raval and Veeraswamy, 2000; Veeraswamy and Raval, 2004; Koptev et al., 2015). The hydrothermal circulation of melts and fluids generated during the plume interaction may result in the reworking of various lithospheric processes. The previous MT, DSS, and geopotential studies suggest magmatic underplating and crustal thinning beneath the CRB (Kaila et al., 1990; Tewari et al., 1991; Mishra et al., 1998; Danda et al., 2017, 2020, 2021). The crystallization of underplating magma generates exsolved fluids causing the occurrence of conducive anomalies (C3-C4) within the CRB crust. The upper mantle conductor (UMC) beneath the conductive anomalies (C3-C4) infers the generation of volatile enriched melts (CO_2, H_2O) and their channelization to crustal depths. Danda et al. (2020, 2021) have attempted to calculate the melt percentage fraction to generate the observed conductivity values in the upper mantle depths. It is inferred that 0.75–3.5% of melt fraction is required to generate such conductivity ranges in the upper mantle. The high heat flow values, and drop in shear velocity suggest the existence of volatile enriched melts in the CRB (Verma et al., 1968; Gupta, 1981; Thiagarajan et al., 2001; Kumar et al., 2016). The Réunion mantle plume interaction has generated such volatile enriched melts, causing the alterations in regional lithospheric structure across western India, such as KRB (Abdul Azeez et al., 2021), Saurashtra (Kumar et al., 2018), NRB (Patro and Sarma, 2016). The regional seismological studies suggest low V_p/V_s velocities in the upper mantle lithosphere across western India due to Deccan volcanism associated with the Réunion plume interaction (Kennett and Widiyantoro, 1999; Sharma et al., 2018; Mandal, 2019; Singh et al., 2019).

The ADFB represents a Precambrian tectonic trend in western India. The present study delineates crust and mantle lithospheric units of the Aravalli-Delhi fold belt as resistive formations (R3-R4). The previous MT studies also showed a similar range of resistivity values for these structural units of ADFB (Danda et al., 2017, 2020, 2021). The Bouguer gravity anomaly along the profile shows a decrement from resistive feature R3 (beneath site no: 17) to the centre of R4 (beneath site no: 25) and becomes almost flat (Fig. 5a& 5b). This decrement in Bouguer gravity anomaly correlates with the transition between resistive features R3 and R4 and might represent a shear zone or a boundary between two different trends within the ADFB. The depth slice at 30 km shows that resistive features R3 and R4 are a single identical block whereas in the slices at 40 and 50 km it appears as two different blocks (Fig. 7). The previous geophysical studies suggest extension of NE-SW Aravalli trend into Saurashtra beneath the CRB, E-W Delhi trend into KRB, and ENE-WSW Satpura trend into NRB (Biswas, 1987; Tewari et al., 1995). We infer that these trends appear as two independent resistive features in the present model. The resistive feature R3 indicates the extension of NE-SW Aravalli trend into the Saurashtra with similar range of resistivity values (Kumar et al., 2018) and corroborates with previous geophysical studies (Biswas, 1987, Tewari et al., 1995). The resistive feature R4 might represent the extension of ENE-WSW Saptura trend into the NRB and it needs to be verified by extending MT studies further south into the ADFB. The steeply dipping shear belt separating Archaean-Proterozoic blocks (between R3 and R4) may sole down to sub horizontal horizon, the bend at lower crustal depths provides favourable pockets, imaged as high conducting zones (C5-C6), for trapping fluids expelled from recrystalising volcanic magmatic intrusion or deposition of sulphide mineralization. The conductive anomalies (C5-C6) infer the deposition Aravalli-Delhi sediments/metasediments, trapped fluids, and sulphide mineralization occurred during the different stages of metamorphism (Danda et al., 2017, 2020, 2021).

4.3. Spatially heterogeneous lithosphere

The lithospheric structure of the CRB is highly heterogenous in nature. The previous MT studies (Danda et al., 2020, 2021) across the CRB have postulated an assemblage of Archaean and Proterozoic lithospheres. Danda et al. (2021) have also made a comparison of the Archaean and Proterozoic resistivity values with global Archaean and Proterozoic to substantiate its assemblage beneath the CRB. The present study delineates a contact of highly resistive (R1) and conductive formations (C3 and UMC) interpreted as the contact between the Archaean (resistive) and Proterozoic (conductive) lithospheres. As discussed in the previous section, channelization of volatile melts into crustal depths due to heat exchange caused by thermal anomaly associated with Réunion plume occurred through the weak Proterozoic lithosphere. The Proterozoic lithosphere is more vulnerable to the interaction of Réunion mantle plume due to its weak nature and its second stage evolution of the CRB which is considered to be coeval with the Deccan volcanism. The depth slice at 40 km shows a clear contact of both lithospheres in terms of resistivity contrast in the southern part (Fig. 7). The Proterozoic become less prominent in the northern part due to the extension of Aravalli trend and uplifted Precambrian crust beneath the Tharad and Diyodar ridges. The conductive Proterozoic lithosphere in the northern part becomes wider and clear at the depth slice of 50 km. The previous MT studies have provided the evidences for heterogeneity as contact of Archaean and Proterozoic lithospheric structures across the CRB (Danda et al., 2020, 2021). The present study highlights the demarcation of spatial heterogeneity in the northern and southern parts of the CRB lithosphere though the extension of NE-SW Aravalli trend into the Saurashtra.

4.4. Comparison of vertically integrated conductance with Bouguer anomaly

We have computed the vertically integrated conductance (from surface to the model depth of 80 km common for all profiles) values by taking the cell thickness from the model grid used for the 2D inversion and its corresponding conductivity for each independent profile. These conductance values on the log10 scale are then contoured after applying one-pass 3-node Gaussian filter smoothing (Fig. 8). We compare this conductance map with the Bouguer gravity anomaly (BGA) map of the study area. Broadly, the BGA and the conductance patterns show some similarity. The ADFB is associated with low conductance and low BGA values (Fig. 8b & c). This positive correlation between the conductance and the BGA values implies the presence of felsic material dominant Archaean gneisses and granites. The conductance map dominantly exhibits moderate to high conductance for both the Archaean and the Proterozoic lithospheres beneath the CRB associated with positive to negative BGA values, respectively (Fig. 8c). Since the CRB and KRB in the study area consist of thick conductive sediments (~2–7 km), we removed the sediment conductance (conductance of the upper 8 km) to obtain the correlation between the BGA and the structures deeper than the basement (Fig. 8d). The deeper structures beneath the CRB exhibit a correlation between low conductance with negative BGA values as seen for the ADFB. The regions of moderate conductance values now correlate with positive BGA. The relatively enhanced conductance and high-density material causing positive BGA possibly represents mafic rocks (Fig. 8d). The variations in the conductance values and the BGA within the CRB also indicate a spatial heterogeneity in the lithospheric structure.

5. Summary and conclusions

Magnetotelluric studies were conducted across the CRB and neighboring KRB and ADFB in western India to map their lithospheric structure for understanding the geodynamic and tectonic evolution of the region and impact of the Réunion mantle plume. Integration of the present and previous MT, DSS, and geopotential results brought out the comprehensive basement and lithospheric structure of the CRB and adjoining regions. The study demarcated different blocks within the CRB, namely, Sanchore, Patan, and Mehsana depressions and Tharad,

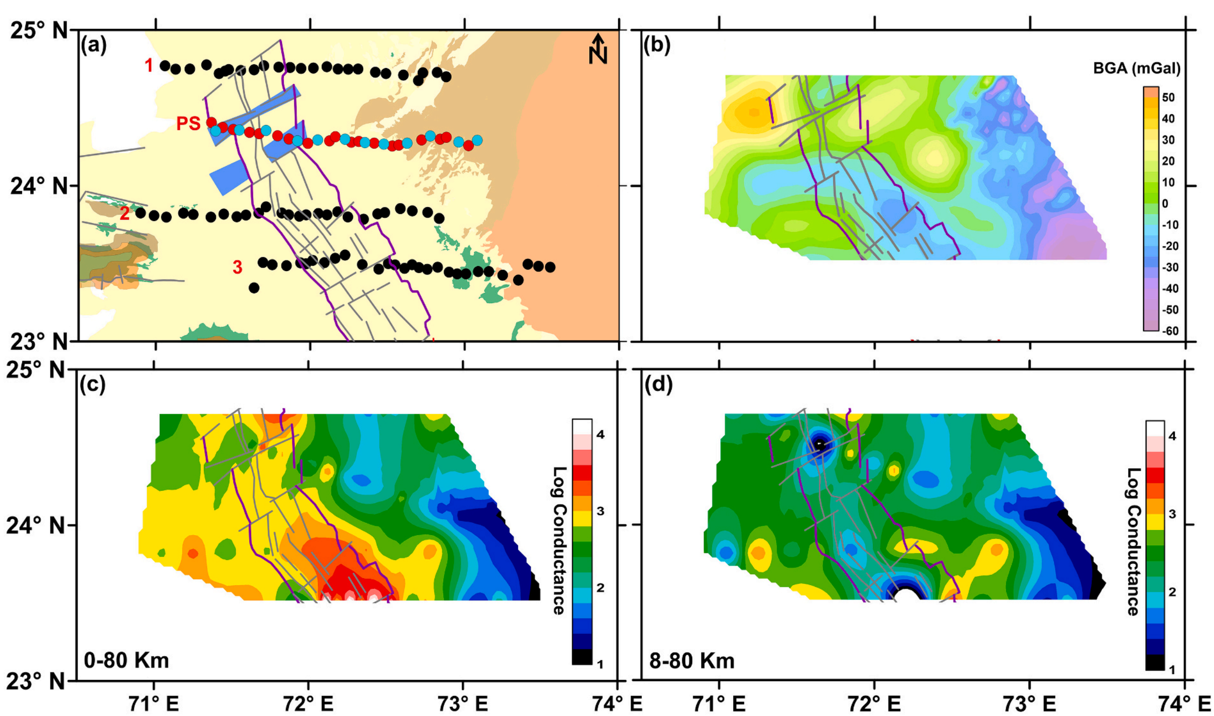

Fig. 8. a) The geological map of study area. The numbers 1,2,3 indicates MT profiles by Danda et al., 2017, 2021, 2020, respectively, and black solid circles represent corresponding MT sites. b) Bouguer gravity contour map over the CRB. c) Vertically integrated conductance for depths 0–80 km. d) Vertically integrated conductance for the depths 8-80 km after removal of sediments conductance over the study region.

and Diyodar ridges with a variation in sedimentary thickness and a slight shift of the eastern boundary of the CRB. The study imaged the basic/ultrabasic intrusives, uplifted Precambrian crust in the CRB, and structural units of the ADFB as resistive formations. The occurrence of sulphide mineralization during various phases of metamorphism and Aravalli-Delhi sediments/metasediments appeared as conductive pockets in the ADFB. The thermal anomaly associated with the Réunion plume generated volatile melts/fluids, and its channelization enhanced the conductivity of the crust and mantle lithosphere beneath the CRB. The Archaean and Proterozoic geological contact beneath the CRB plays a significant role in channelization through the weak Proterozoic lithosphere. Further, the comparison of vertically integrated conductance with BGA highlights the spatially heterogeneous lithosphere beneath the Patan-Sanchore to Ahmedabad-Mehsana blocks in the northern part the CRB. It is interpreted that the highly resistive depleted Archaean lithosphere indicates the initial stage of CRB rifting whereas conductive Proterozoic lithosphere represents the second stage of rifting coeval with the Deccan volcanism.

Declaration of Competing Interest

The authors declare that they have no known competing financial interests or personal relationships that could have appeared to influence the work reported in this paper.

Data availability

Data will be made available on request.

Acknowledgements

We are grateful to Ministry of Earth Sciences (MoES), Government of India, for financial support through the project MoES/P.O.(Seismo)/1 (130)/2011 to take up this study. Authors are grateful to Drs. P.B.V. Subba Rao and A.K. Singh, Indian Institute of Geomagnetism (IIG) for participation in the data acquisition. ND is thankful to Department of Science and Technology, Government of India for a Ph.D. fellowship to pursue research work at IIG, and to Council of Scientific and Industrial Research (CSIR) for a Research Associate fellowship (Grant number: 31/0023(13135)/2021-EMR-1) to carry out post-doctoral work at CSIR-National Geophysical Research Institute (CSIR-NGRI). Michael Becken is acknowledged for providing his MT-strike code. Thanks to the Director IIG, and the Director, CSIR-NGRI, for their kind permissions and necessary approvals to publish this work. We thank the Editor, Dr. Ramon Carbonell and two anonymous reviewers for their insightful comments that have helped in improving the manuscript.

Appendix A. Supplementary data

Supplementary data to this article can be found online at https://doi.org/10.1016/j.tecto.2023.229905.

References

Abdul Azeez, K.K., Mohan, K., Veeraswamy, K., Rastogi, B.K., Gupta, A.K., Harinarayana, T., 2018. 3D crustal resistivity structure beneath the Wagad aftershock zone of the 2001 Bhuj earthquake, Kutch, India: heterogeneous resistivity structure controlled by widespread fluid infiltration and clues to aftershocks pattern. Tectonophysics 747–748, 54–67.

Abdul Azeez, K.K., Mohan, K., Veeraswamy, K., Rastogi, B.K., Gupta, A.K., Harinarayana, T., 2021. Lithospheric resistivity structure of the 2001 Bhuj earthquake aftershock zone. Geophys. J. Int. 224, 1980–2000.

Adilakshmi, L., Manglik, A., Thiagarajan, S., Suresh, M., 2021. Crustal structure of the Indian plate underneath the alluvial plains of the central Ganga basin by broadband magnetotellurics. Tectonophysics 802, 228746.

Becken, M., Burkhardt, H., 2004. An ellipticity criterion in magnetotelluric tensor analysis. Geophys. J. Int. 159, 69–82.

Bhatacharji, S., Chatterjee, N., Wampler, J.M., Nayak, P.N., Deshmukh, S.S., 1996. Indian intraplate and continental margin rifting, lithospheric extension, and mantle upwelling in Deccan flood basalt volcanism near the K/T boundary: evidence from mafic dike swarms. J. Geol. 104, 379–398.

Biswas, S.K., 1982. Rift basins in the western margin of India and their hydrocarbon prospects. Bull. Am. Assoc. Pet. Geol. 66, 1497–1513.

Biswas, S.K., 1987. Regional tectonic framework, structure and evolution of the western marginal basins of India. Tectonophysics 135, 307–327.

Brasse, H., Lezaeta, P., Rath, V., Schwalenberg, K., Soyer, W., Haak, V., 2002. The Bolivian Altiplano conductivity anomaly. J. Geophys. Res. 107 (B5), 2096.

Burke, K.C., Dewey, J.F., 1973. Plume-generated triple junctions: key indicators in applying plate tectonics to old rocks. J. Geol. 81, 403–433.

Caldwell, T.G., Bibby, H.M., Brown, C., 2004. The magnetotelluric phase tensor. Geophys. J. Int. 158, 457–469.

Chave, A.D., Thomson, D.J., 2004. Bounded influence magnetotelluric response function estimation. Geophys. J. Int. 157, 988–1006. https://doi.org/10.1111/j.1365-246X.2004.02203.x.

Chouhan, A.K., Choudhury, P., Pal, S.K., 2020. New evidence for a thin crust and magmatic underplating beneath the Cambay rift basin, Western India through modelling of EIGEN-6C4 gravity data. J. Earth Syst. Sci. 129, 64.

Comeau, M.J., Käuflb, S.J., Becken, M., Kuvshinov, A., Grayver, A.V., Kamm, J., Demberel, S., Sukhbaatar, U., Batmagnai, E., 2018. Evidence for fluid and melt generation in response to an asthenospheric upwelling beneath the Hangai Dome, Mongolia. Earth Planet. Sci. Lett. 487, 201–209.

Courtillot, V., Fraud, G., Maluski, H., Vandamme, D., Moreau, M.G., Besse, J., 1988. Deccan flood basalts and the Cretaceous–Tertiary boundary. Nature 333, 843–846.

Danda, N., Rao, C.K., 2019. Magnetotelluric study to characterize sediment thickness across Kachchh and Cambay rift basins, western India. Curr. Sci. 116, 299–304.

Danda, N., Rao, C.K., Kumar, A., 2017. Geoelectric structure of northern Cambay rift basin from magnetotelluric data. Earth Planets Space 69, 140.

Danda, N., Rao, C.K., Kumar, A., Rama Rao, P., Subba Rao, P.B.V., 2020. Implications for the lithospheric structure of Cambay rift zone, western India: Inferences from a magnetotelluric study. Geosci. Front. 11, 1743–1754.

Danda, N., Rao, C.K., Pavankumar, G., Kumar, A., Manglik, A., 2021. Magnetotelluric evidence for an Archaean – Proterozoic lithospheric assemblage within the Cambay rift basin, western India, and its role in channeling of plume-derived fluids within the basin. Tectonophysics 818, 229064.

Dewey, J.F., Ryan, P.D., Andersen, T.B., 1993. Orogenic uplift and collapse, crustal thickness, fabrics and metamorphic phase changes: The role of eclogies, in Magmatic Processes and Plate Tectonics, 76, 325–343. In: Prichard, H.M., Alabaster, T., Harris, N.B.W., Neary, C.R. (Eds.), Geol. Soc. of London Spec. Publ.

Dixit, M.M., Tewari, H.C., Rao, C.V., 2010. Two-dimensional velocity model of the crust beneath the South Cambay Basin, India from refraction and wide-angle reflection data. Geophys. J. Int. 181, 635–652.

Dunbar, J.A., Sawyer, D.S., 1989. Continental rifting at pre-existing lithospheric weaknesses. Nature 242, 565–571.

Duncan, R.A., Pyle, D.G., 1988. Rapid eruption of the Deccan flood basalts at the cretaceous/Tertiary boundary. Nature 333, 841–843.

Gamble, T.D., Goubau, W.M., Clarke, J., 1979. Magnetotellurics with a remote magnetic reference. Geophys. 44, 53–68.

GEBCO Compilation Group, 2021. GEBCO 2021 Grid. https://doi.org/10.5285/c6612cbe-50b3-0cff-e053-6c86abc09f8f.

Griffiths, R.W., Campbell, I.H., 1990. Stirring and structure in mantle starting plumes. Earth Planet. Sci. Lett. 99, 66–78.

Gupta, M.L., 1981. Surface heat flow and igneous intrusion in the Cambay Basin, India. J. Volcanol. Geotherm. Res. 10, 279–292.

Hyndman, R.D., Shearer, P.M., 1989. Water in the lower continental crust: modelling magnetotelluric and seismic reflection results. Geophys. J. Int. 98, 343–365.

Jones, A.G., 1983. The problem of current channeling: a critical review. Geophys. Surv., (now Surv. Geophys.) 6, 79–122.

Jones, A.G., Jödicke, H., 1984. Magnetotelluric transfer function estimation improvement by a coherence-based technique. In: Proceedings of 54th Annual International Meeting of Society of Explorations Geophysics, Atlanta, GA, Dec 2–6.

Jones, A.G., Chave, A.D., Auld, D., Bahr, K., Egbert, G., 1989. A comparison of techniques for magnetotelluric response function estimation. J. Geophys. Res. 94, 14201–14213.

Kaila, K.L., Krishna, V.G., Mall, D.M., 1981. Crustal structure along Mehmadabad-Billimora profile in the Cambay basin, India, from deep seismic soundings. Tectonophysics 76, 99–130.

Kaila, K.L., Tewari, H.C., Krishna, V.G., Dixit, M.M., Sarkar, D., Reddy, M.S., 1990. Deep seismic sounding studies in the North Cambay and Sanchore basins, India. Geophys. J. Int. 103, 621–637.

Kennett, B.L.N., Widiyantoro, S., 1999. A low seismic wave speed anomaly beneath northwestern India: a seismic signature of the Deccan plume? Earth Planet. Sci. Lett. 165, 145–155.

Koptev, A., Calais, E., Burov, E., Leroy, S., Gerya, T., 2015. Dual continental rift systems generated by plume–lithosphere interaction. Nat. Geosci. 8, 388–392.

Kumar, P., Sen, G., Mandal, P., Sen, M.K., 2016. Shallow lithosphere–asthenosphere boundary beneath Cambay Rift Zone of India: inferred presence of carbonated partial melt. J. Geol. Soc. India 88, 401–406.

Kumar, V.V.P., Patro, P.K., Subba Rao, P.B.V., Singh, A.K., Kumar, A., Nagarjuna, D., 2018. Electrical resistivity cross-section across northern part of Saurashtra region: an insight to crystallized magma and fluids. Tectonophysics 744, 205–214.

Ledo, J., 2005. 2D versus 3D magnetotelluric data interpretation. Surv. Geophys. 26, 671–806.

Ledo, J., Queralt, P., Marti, A., Jones, A.G., 2002. Two-dimensional interpretation of three-dimensional magnetotelluric data: an example of limitations and resolution. Geophys. J. Int. 150, 127–139.

Ledo, J., Jones, A.G., Ferugson, I.J., Wolynec, L., 2004. Lithospheric structure of the Yukon, northern Canadian Cordillera, obtained from magnetotelluric data. J. Geophys. Res. 109, B04410.
Liang, H., Jin, S., Wei, W., Gao, R., Ye, G., Zhang, L., Yin, Y., Lu, Z., 2018. Lithospheric electrical structure of the middle Lhasa terrane in the south Tibetan plateau. Tectonophysics 731–732, 95–103. https://doi.org/10.1016/j.tecto.2018.01.020.
Mackie, R., Rieven, S., Rodi, W., 1997. Users Manual and Software Documentation for Two-Dimensional Inversion of Magnetotelluric Data. GSY-USA, Inc., San Francisco, California.
Mahoney, J., Nicollet, C., Dupuy, C., 1991. Madagascar basalts: Tracking oceanic and continental sources. Earth Planet. Sci. Lett. 104 (2–4), 350–363.
Mandal, P., 2019. A possible origin of intraplate earthquakes in the Kachchh rift zone, India, since the 2001 Mw7.7 Bhuj earthquake. J. Asian Earth Sci. 170, 56–72.
McKenzie, D., 1985. The extraction of magma from the crust and mantle. Earth Planet. Sci. Lett. 74, 81–91.
Meissner, R., Wever, Th., Sadowiak, P., 1991. Continental collisions and seismic signature. Geophys. J. Int. 105, 15–23. https://doi.org/10.1111/j.1365-246X.1991.tb03440.x.
Merh, S.S., 1995. Geology of Gujarat. Geological Society of India Publication, Bangalore, pp. 1–170.
Mishra, D.C., Gupta, S.B., Tiwari, V.M., 1998. A geotransect from Dharimanna to Billimora across the Cambay and Narmada-Tapti rift basins, India. Int. Geol. Rev. 40, 1007–1020.
Morgan, W.J., 1971. Convection plumes in the lower mantle. Nature 230, 42–43.
Morgan, W.J., 1981. Hotspot Tracks and the Opening of the Atlantic and Indian Oceans. Wiley, New York, pp. 443–487.
Ogawa, Y., 2002. On two-dimensional modeling of magnetotelluric field data. Surv. Geophys. 23, 251–273.
Patro, P.K., Sarma, S.V.S., 2016. Evidence for an extensive intrusive component of the Deccan large Igneous Province in the Narmada Son Lineament region, India from three dimensional magnetotelluric studies. Earth Planet. Sci. Lett. 451, 168–176.
Pavankumar, G., Manglik, A., 2011. Effect of Himalayan topography on two-dimensional interpretation of magnetotelluric data. Curr. Sci. 100 (3), 390–395.
Pavankumar, G., Manglik, A., Thiagarajan, S., 2014. Crustal Geoelectric structure of Sikkim Himalaya and adjoin Gangetic foreland basin. Tectonophysics 637, 238–250.
Pavankumar, G., Mahesh, P., Nagar, M., Mahender, E., Kumar, V., Mohan, K., Kumar, M. R., 2017. Role of deep crustal fluids in the genesis of intraplate earthquakes in the Kachchh region, northwestern India. Geophys. Res. Lett. 44, 4054–4063.
Rao, C.K., Jones, A.G., Moorkamp, M., Weckmann, U., 2014. Implications for the lithospheric geometry of the Iapetus suture beneath Ireland based on electrical resistivity models from deep-probing magnetotellurics. Geophys. J. Int. 198, 737–759.
Rao, K.M., Kumar, M.R., Rastogi, B.K., 2015. Crust beneath the northwestern Deccan Volcanic Province, India: evidence for uplift and magmatic underplating. J. Geophys. Res. Solid Earth 120, 3385–3405.
Raval, U., Veeraswamy, K., 2000. The radial and linear modes of interaction between mantle plume and continental lithosphere: a case study from western India. J. Geol. Soc. India 56, 525–536.
Rodi, W., Mackie, R.L., 2001. Nonlinear conjugate gradients algorithm for 2D magnetotelluric inversion. Geophys. 66, 174–187.
Saunders, A.D., Storey, M., Kent, R.W., Norry, M.J., 1992. Consequences of plume-lithosphere interactions. Geol. Soc. Lond., Spec. Publ. 68, 41–60. https://doi.org/10.1144/GSL.SP.1992.068.01.04.
Schmoldt, J.P., Jones, A.G., Rosell, O., 2014. Structures and geometries of the Tajo Basin crust, Spain: results of a magnetotelluric investigation compared to seismic and thermal models. Tectonics 33 (9), 1710–1737.
Schwalenberg, K., Rath, V., Haak, V., 2002. Sensitivity studies applied to a two-dimensional resistivity model from the Central Andes. Geophys. J. Int. 150 (3), 673–686.
Sharma, J., Kumar, M.R., Roy, K.S., Roy, P.N.S., 2018. Seismic imprints of plume-lithosphere interaction beneath the northwestern Deccan Volcanic Province. J. Geophys. Res. Solid Earth 123, 10,831–10,853.
Singh, A.P., Koulakov, I., Kumar, M.R., Kumar, S., Kayal, J.R., 2019. Seismic velocity structure and intraplate seismicity beneath the Deccan Volcanic Province of western India. Phys. Earth Planet. Inter. 287, 21–36.
Tewari, H.C., Dixit, M.M., Sarkar, D., Kaila, K.L., 1991. A crustal density model across the Cambay basin, India, and its relationship with the Aravallis. Tectonophysics 194, 123–130.
Tewari, H.C., Dixit, M.M., Sarkar, D., 1995. Relationship of the Cambay rift basin to the Deccan volcanism. J. Geodyn. 20, 85–95.
Thiagarajan, S., Ramana, D.V., Rai, S.N., 2001. Seismically constrained two-dimensional crustal thermal structure of the Cambay basin. J. Earth Syst. Sci. 110, 1–8.
Varentsov, I.M., Sokolova, E.Y., Martanus, E., Nalivaiko, K., BEAR Working Group, 2003. System of electromagnetic field transfer operators for the BEAR array of simultaneous soundings: methods and results. Izv. Phys. Solid Earth 39, 118–148.
Veeraswamy, K., Raval, U., 2004. Chipping of cratons and breakup along mobile belts of a supercontinent. Earth Planets Space 56, 491–500.
Verma, R.K., Gupta, M.L., Hamza, V.M., Rao, G.V., Rao, R.U.M., 1968. Heat flow and crustal structure near Cambay, Gujarat, India. Bull. Natl. Geophys. Res. Inst. 6, 153–166.
Wannamaker, P.E., Hohmann, G.W., Ward, S.H., 1984. Magnetotelluric responses of 3 dimensional bodies in layered Earths. Geophys. 49, 1517–1533.
Watts, A.B., Cox, K.G., 1989. The Deccan Traps: an interpretation in terms of progressive lithospheric flexure in response to a migrating load. Earth Planet. Sci. Lett. 93 (1), 85–97. https://doi.org/10.1016/0012-821X(89)90186-6.
White, R.S., McKenzie, D.P., 1989. Magmatism at rift zones: the generation of volcanic continental margins and flood basalts. J. Geophys. Res. 94, 7685–7729.
Worzewski, T., Jegen, M., Kopp, H., Brasse, H., Castillo, W.T., 2011. Magnetotelluric image of the fluid cycle in the Costa Rican subduction zone. Nat. Geosci. 4, 108–111.
Yardley, B.W.D., Bodnar, R.J., 2014. Fluids in the continental crust. Geochem. Perspect. 3, 1–127.